Optics Communications 410 (2018) 977–982

Contents lists available at ScienceDirect

Optics Communications

journal homepage: www.elsevier.com/locate/optcom

Optical illusions induced by rotating medium

XiaoFei Zang [a,b], PengCheng Huang [a], YiMing Zhu [a,b,*]

[a] Shanghai Key Lab of Modern Optical System, University of Shanghai for Science and Technology, Shanghai 200093, PR China
[b] Terahertz Science Cooperative Innovation Center, Chengdu 610054, PR China

ARTICLE INFO

Keywords:
Transformation optics
Rotating medium
Super-resolution effects
Illusion optics

ABSTRACT

Different from the traditional single-function electromagnetic wave rotators (rotate the electromagnetic wavefronts), we propose that rotating medium can be extended to optical illusions such as breaking the diffraction limit and overlapping illusion. Furthermore, the homogeneous but anisotropic rotating medium is simplified by homogeneous and isotropic positive-index materials according to the effective medium theory, which is helpful for future device fabrication. Finite element simulations for the two-dimensional case are performed to demonstrate these properties.

1. Introduction

Transformation optics (TO), proposed by U. Leonhardt and J. B. Pendry, respectively [1,2], is one of the most well-known theories to manipulate electromagnetic waves. One important application is the invisible cloak. In recent years, many kinds of cloaks, such as cylindrical cloak, square cloak, elliptic cloak, arbitrary shaped cloak, cloak of twisted domain, open cloak, the general open-closed cloak, complementary cloak, and so on have been theoretically studied [3–16]. Meanwhile, experimental verifications of invisible cloaks ranging from microwave to visible frequency have been also reported [17–23]. Besides the application of invisible cloak, TO can also be applied to design other kinds of devices, i.e., beam splitter, high-directional emission, electromagnetic black-hole, super-scatterers, tunable electromagnetic gateways, overlapped optics, *etc.* [24–36].

Recently, Chen and Chan have proposed electromagnetic waves (EM) rotator, where electromagnetic fields were rotated for a fixed angle, can give rise to a rotated world to the observers inside/outside the rotation coating [37]. Subsequently, the cylindrical micro-wave field rotators were experimentally realized. But the proposed of EM rotators suffered from the complex and inhomogeneous material parameters [38,39]. Then, Han et al. proposed a polygonal rotator with homogeneous, nonmagnetic, and isotropic materials, which is more feasible for future realization [40]. Up to now, all of the reported rotators mainly focused on one specific function—rotating the EM wavefronts. In other words, researchers usually think that EM rotator just provides only single function of rotating. Does it has any other kinds of functions or can we develop other new types of functions based on EM rotator?

Here, we have proved that EM rotator can be applied to realize optical illusions such as breaking the diffraction limit and overlapping illusion, simultaneously. This means that EM rotator can not only rotate the EM wavefronts but also be extended to break the diffraction limit and overlapping illusion, resulting in a multi-functional (tri-functional) device. Furthermore, based on the effective medium theory, we simplified the transformation medium, which is isotropic but homogeneous with positive permittivity and permeability. All of the functions of EM rotator are demonstrated by using the two-dimensional finite element simulation. We want to emphasis that in traditional case, the effects of (TO-based) breaking diffraction limit and overlapping illusion can't be realized simultaneously in just one transformation device. That is to say, two different kinds of transformation medium *i.e.*, complementary medium and shifting/compression medium [29,32,35] are needed to realize these two physical phenomena. In this paper, we mainly demonstrate that the positive-index rotating medium is designed to realize the effects of breaking the diffraction limit as well as overlapping illusion, simultaneously.

2. Theory

Fig. 1 schematically depicts the structure of a pentagon EM rotator in the cartesian coordinate system. Each side region consists of two triangles, embedded with different transformation medium. Here, the function of our pentagon EM rotator is to rotate the wavefronts and keep itself invisible. So, we must keep the outer boundary unchanged but rotate the inner boundary. The external triangle $\Delta a_i' a_{i+1}' b_i'$ and internal

* Corresponding author at: Shanghai Key Lab of Modern Optical System, University of Shanghai for Science and Technology, Shanghai 200093, PR China.
E-mail address: ymzhu@usst.edu.cn (Y. Zhu).

http://dx.doi.org/10.1016/j.optcom.2017.08.038
Received 16 May 2017; Received in revised form 15 August 2017; Accepted 17 August 2017
Available online 17 September 2017
0030-4018/

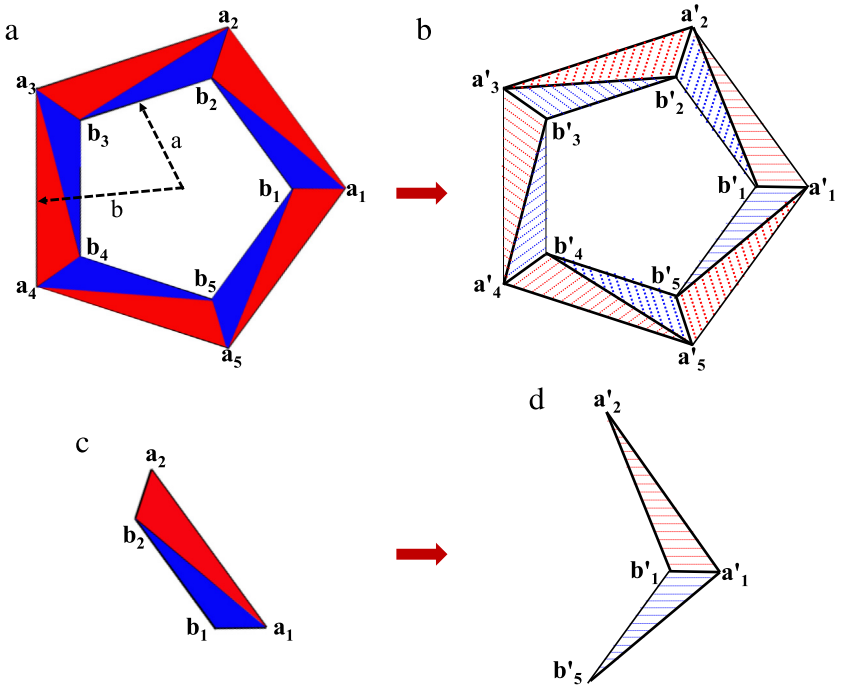

Fig. 1. Schematic of pentagon electromagnetic wave rotator. (a) real space; (b) virtual space; the red (blue) region in (a) is mapped into the red dash line (blue dash line) region in (b). (c) and (d) are the corresponding coordinate mapping between region $a_1a_2b_2b_1$ and $a'_1a'_2b'_1b'_5$: region $a_1a_2b_2$ ($a_1b_2b_1$) is mapped into region $a'_1a'_2b'_1$ ($a'_1b'_1b'_5$). The coordinate mapping of the other regions in (a) and (b) is the same as (c) and (d). (For interpretation of the references to color in this figure legend, the reader is referred to the web version of this article.)

triangle $\Delta a'_i b'_i b'_{i-1}$ in virtual space are mapping into $\Delta a_i a_{i+1} b_{i+1}$ and $\Delta a_i b_{i+1} b_i$in real space, respectively [37]. Taking the region $a_1a_2b_2b_1$as an example, the corresponding coordinate mapping between the virtual space and real space is by transforming $\Delta a'_1 a'_2 b'_1$ and $\Delta a'_1 b'_1 b'_5$ in virtual space into $\Delta a_1 a_2 b_2$ and $\Delta a_1 b_2 b_1$ in real space with the point-to-point mapping as follows:

$$\begin{cases} a_1 \leftrightarrow a'_1 \\ a_2 \leftrightarrow a'_2 \\ b_2 \leftrightarrow b'_1 \end{cases}, \qquad \begin{cases} a_1 \leftrightarrow a'_1 \\ b_2 \leftrightarrow b'_1 \\ b_1 \leftrightarrow b'_5 \end{cases}.$$

The general expression of the ith vertex in Fig. 1 can be defined as:

$$\begin{aligned} x_{a_i} &= a\cos\left[(i-1)\,2\pi/5\right], \\ y_{a_i} &= a\sin\left[(i-1)\,2\pi/5\right], \\ x_{b_i} &= b\cos\left[(i-1)\,2\pi/5\right], \\ y_{b_i} &= b\sin\left[(i-1)\,2\pi/5\right], \end{aligned} \tag{1}$$

where $1 \le i \le 5$, and $a(b)$ is the corresponding distance between the center of the device and $a_i(b_i)$.

For the external triangles, the corresponding coordinate transformation is expressed as:

$$\begin{aligned} x &= m_1 x' + m_2 y' + m_3, \\ y &= n_1 x' + n_2 y' + n_3, \\ z &= z', \end{aligned} \tag{2}$$

where $\begin{bmatrix} m_1 n_1 \\ m_2 n_2 \\ m_3 n_3 \end{bmatrix} = A^{-1} \begin{bmatrix} x_{a_i} & y_{a_i} \\ x_{a_{i+1}} & y_{a_{i+1}} \\ x_{b_{i+1}} & y_{b_{i+1}} \end{bmatrix}$, and $A = \begin{bmatrix} x_{a_i} & y_{a_i} & 1 \\ x_{a_{i+1}} & y_{a_{i+1}} & 1 \\ x_{b_i} & x_{b_{i+1}} & 1 \end{bmatrix}$.

For the internal triangles, the corresponding coordinate transformation can be written as:

$$\begin{aligned} x &= p_1 x' + p_2 y' + p_3, \\ y &= q_1 x' + q_2 y' + q_3, \\ z &= z', \end{aligned} \tag{3}$$

where $\begin{bmatrix} p_1 q_1 \\ p_2 q_2 \\ p_3 q_3 \end{bmatrix} = B^{-1} \begin{bmatrix} x_{a_i} & y_{a_i} \\ x_{b_{i+1}} & y_{b_{i+1}} \\ x_{b_i} & y_{b_i} \end{bmatrix}$, and $B = \begin{bmatrix} x_{a_i} & y_{a_i} & 1 \\ x_{b_i} & y_{b_i} & 1 \\ x_{b_{i-1}} & y_{b_{i-1}} & 1 \end{bmatrix}$.

Actually, there are many kinds of coordinate transformations to realize the mapping shown in Fig. 1. The forms in Eqs. (2) and (3) are similar to quasi-conformal transformations like in [40–44]. Therefore, the corresponding material parameters are not space variant, in which, it can be realized by conventional materials such as uniaxial crystal [45,46].

Based on the above equations, we deduce the expression of the permittivity tensor and permeability.

For the external triangle (Fig. 1(a)):

$$\begin{aligned} \overleftrightarrow{\varepsilon}_{outer} &= \varepsilon_0 \begin{bmatrix} m_1^2 + m_2^2 & m_1 n_1 + m_2 n_2 \\ m_1 n_1 + m_2 n_2 & n_1^2 + n_2^2 \end{bmatrix}, \\ \mu_{outer} &= \mu_0, \end{aligned} \tag{4}$$

For the internal triangle (Fig. 1(a)):

$$\begin{aligned} \overleftrightarrow{\varepsilon}_{inner} &= \varepsilon_0 \begin{bmatrix} p_1^2 + p_2^2 & p_1 q_1 + p_2 q_2 \\ p_1 q_1 + p_2 q_2 & q_1^2 + q_2^2 \end{bmatrix}, \\ \mu_{inner} &= \mu_0. \end{aligned} \tag{5}$$

3. Numerical simulation and discussion

First, the functionality of the field rotating is demonstrated in Fig. 2. The corresponding parameters are as follows: $a = 0.75$ mm, $b = 0.5$ mm and the frequency of the point source is 0.3 THz (the corresponding wavelength (λ) is 1 mm). Fig. 2(a) depicts the magnetic field distribution of a point source located at point b_1 and covered with transformation medium. Fig. 2(b) shows the corresponding magnetic field distribution (in free space) of the identical point source located at point b'_5. Comparing with Figs. 2(a) and 2(b), both of them have the same field distribution outside the rotator, although the field distributions inside the rotators are totally different from each other. It means that the point source located in point b_1 (in the physical space of Fig. 2(a)) and coated with the transformations medium is virtually rotated into point b'_5 in the virtual space (with intersection angle of $\Delta b'_1 o b'_5$ is 72°), demonstrating the rotating feature of our designed field rotator. When

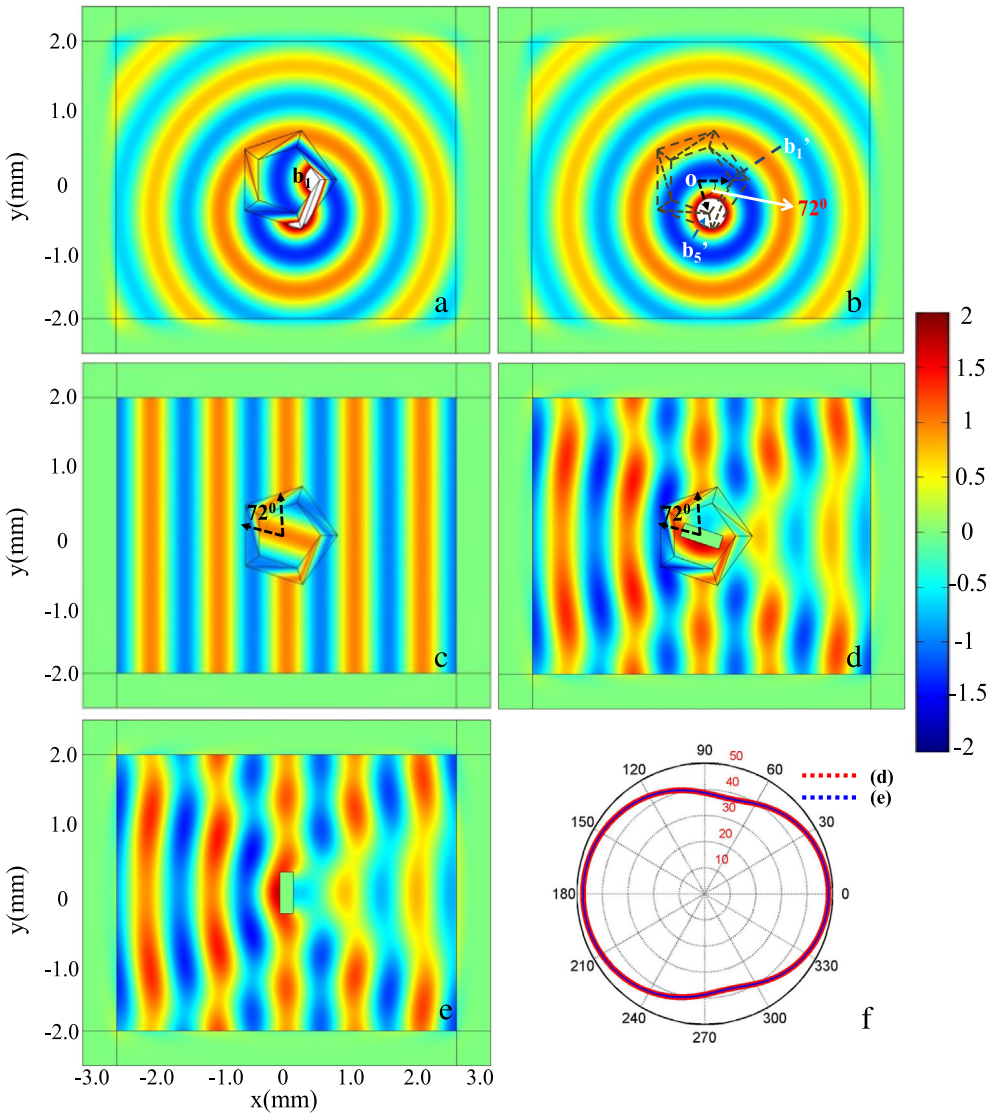

Fig. 2. The magnetic field distributions of a point-source embedded into the transformation medium (a) and free space (b), respectively. The magnetic field distributions of plane-wave propagating from left side without object (c) and with a rectangle PMC (perfect magnetic conductor) (d) inside the region $b_1b_2b_3b_4b_5$. (e) The equivalent magnetic field distributions of (d), when the plane-wave is interacted with a rectangle PMC vertically located in the free space. (f) The corresponding far-field patterns of (d) and (e).

the plane-wave propagates from the left side and interacts with the transformation medium, the magnetic field inside the region $b_1b_2b_3b_4b_5$ is rotated counterclockwise with 72°, as shown in Fig. 2(c). For a rectangle PMC (rotated anticlockwise with 72°to the perpendicular direction) inside the region $b_1b_2b_3b_4b_5$, the corresponding magnetic field distribution and far-field pattern is the same as case of rectangle PMC vertically located in the free space (see Figs. 2(d) –2(e)). It demonstrates that the object inside the inner region of the transformation medium is virtually rotated clockwise with 72°. In a word, the proposed pentagon electromagnetic wave rotator can rotate an object clockwise with 72°. Therefore, the angle difference between the inner region and outside the transformation region is 72°.

Now, we investigate the first application by virtual of the rotating medium. Fig. 3(a) illustrates the magnetic field distribution of two separated identical point sources in free space and located at point a_4' and b_4', respectively. The distance between point $a_4(a_4')$ and $b_4(b_4')$ is 0.25 mm ($\lambda/4$), so, these two separated point sources can't be distinguished due to the diffraction limit. The wavefront of these two separated identical point sources shown in Figs. 3(a) and 3(d) (blue curve) is a circle. Therefore, we can easily break the diffraction limit based on the field rotator as shown in Fig. 3(b). Here, these two separated identical point sources are located at point a_4 and b_4, respectively, and both of them are embedded by the rotating medium. The obviously inhomogeneous strong and weak magnetic field distributions appeared due to the coherent effects, as shown in Fig. 3(b), behaving as beyond the diffraction limit. Fig. 3(c) shows the field distribution of these two separated identical point sources located at point a_4' and b_3', with the separation distance of 0.778 mm (0.778λ). Comparing Figs. 3(b) and 3(c) and the corresponding far-field features in Fig. 3(d) (red and green curves), both of them have the identical field distribution and the far-field features, which demonstrate that these two separated identical point sources coated with rotating medium (with separation distance of 0.25 λ shown in Fig. 3(b)) appeared as breaking the diffraction limit due to the rotating effects. That is to say, in Fig. 3(b), the point source in point b_4 is virtually rotated into point b_3' (in the virtual space), enhancing the distance between these two identical point sources in the virtual space and breaking the diffraction limit.

Then, we study the opposite effects, *i.e.*, the overlapping illusion, also by using such rotating medium. Fig. 4(a) shows the magnetic field distribution of two separated identical point sources located in point a_3' and b_4' (with separation distance of 0.778λ), without any transformation medium. Obviously, these two point sources can be distinguished in the free space. However, when these two point sources are coated with the rotating medium, the wavefront of field distribution

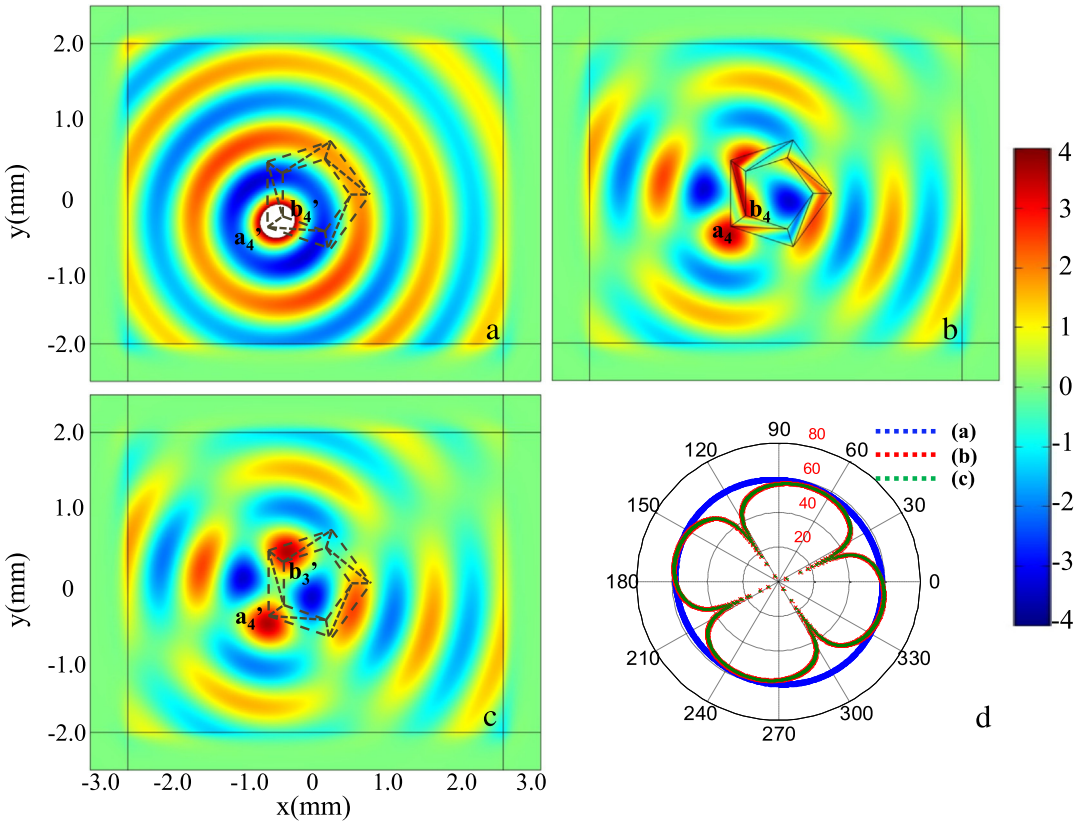

Fig. 3. The magnetic field distribution of two separated point-sources located at point a_4 and b_4 with separation distance of $\lambda/4$ in free space (a) and transformation medium (b). (c) The magnetic field distribution of two separated point-sources located at point a_4 and b_5 with a separation distance larger than 0.778λ in free space. (d) The corresponding far field features of (a) blue curve, (b) red curve and (c) green curve. (For interpretation of the references to color in this figure legend, the reader is referred to the web version of this article.)

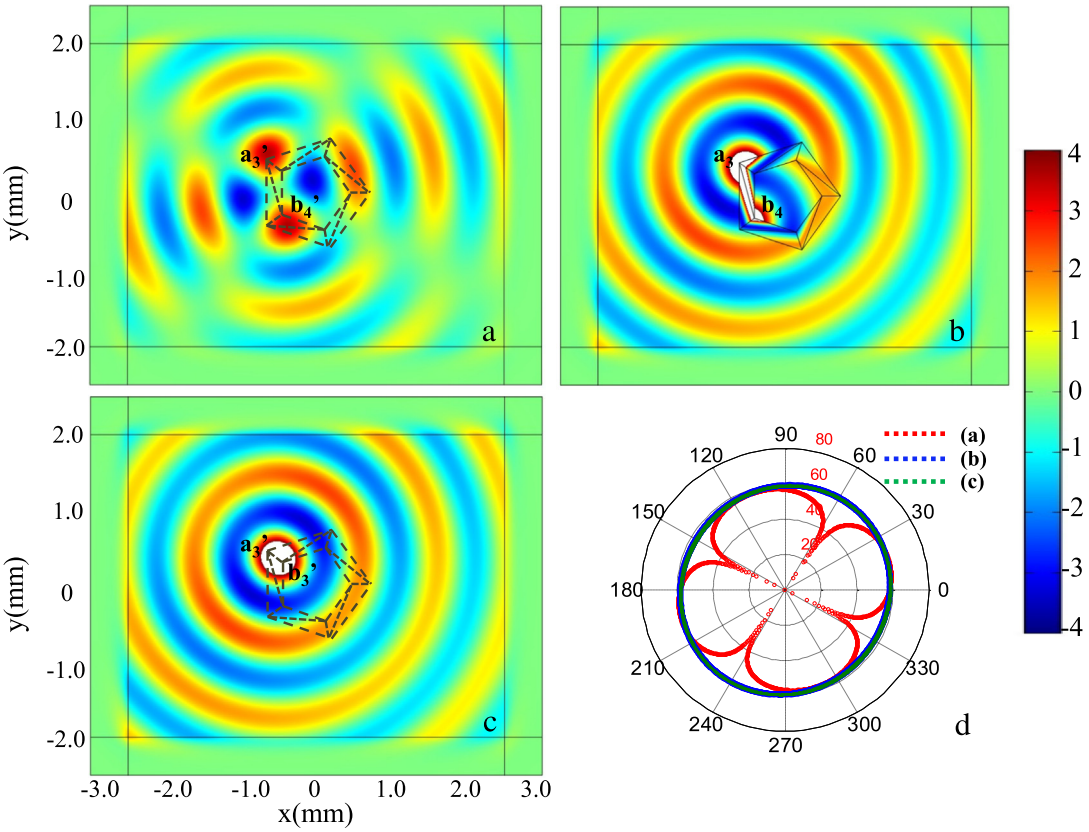

Fig. 4. The magnetic field distribution of two separated point-sources located at point a_3 and b_4 with separation distance of $0.778\ \lambda$ in free space (a) and transformation medium (b). (c) The magnetic field distribution of two separated point-sources located at point a_3 and b_3 with a separation distance larger than $\lambda/4$ in free space. (d) The corresponding far field features of (a) blue curve, (b) red curve and (c) green curve. (For interpretation of the references to color in this figure legend, the reader is referred to the web version of this article.)

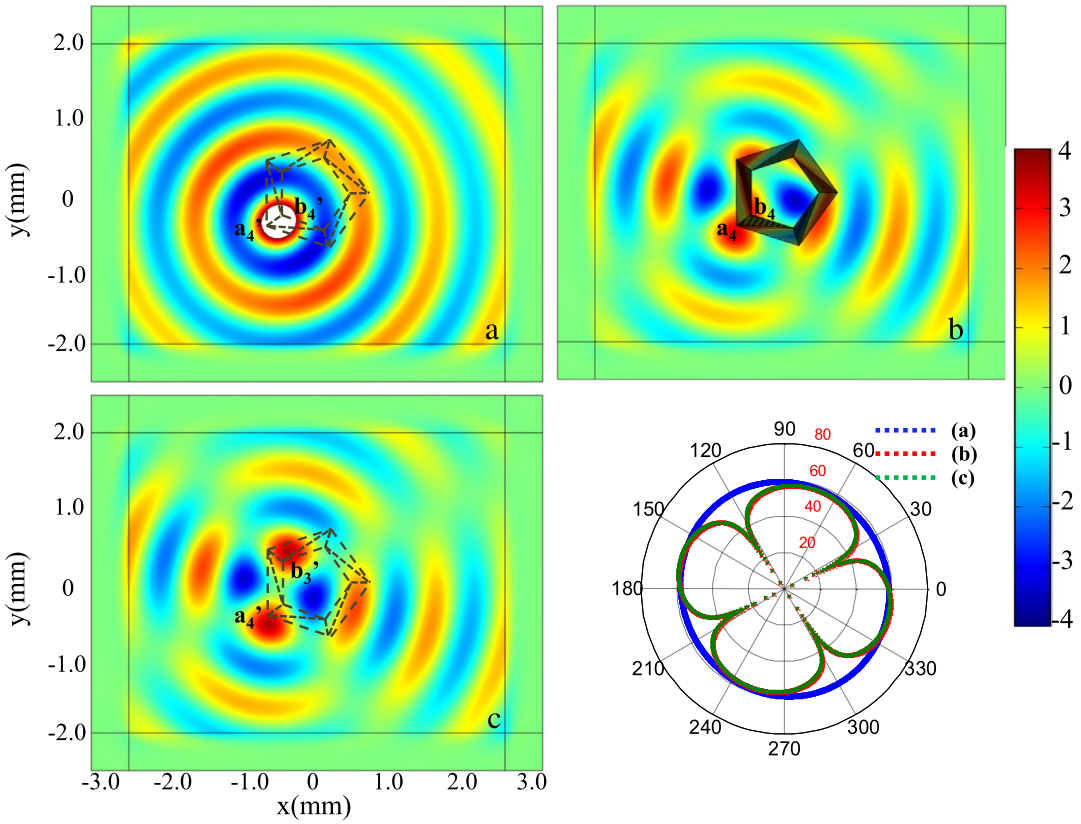

Fig. 5. The magnetic field distribution of two separated point-sources located at point a_4 and b_4 with separation distance of $\lambda/4$ in free space (a) and layered transformation medium (b). (c) The magnetic field distribution of two separated point-sources located at point a_4 and b_3 with a separation distance larger than 0.778λ in free space. (d) The corresponding far field features of (a) blue curve, (b) red curve and (c) green curve. (For interpretation of the references to color in this figure legend, the reader is referred to the web version of this article.)

outside the transformation region (Fig. 4(b)) and the far field feature (Fig. 4(d) of blue curve) are nearly formed as a circle, behaving as a monopole (overlapped with each other). Fig. 4(c) depicts the magnetic field distribution of these two identical point sources located at point a_3' and b_3' with separation distance of 0.25 λ. In Figs. 4(b) and 4(c), both of them have the same field distributions. In other words, the point source in b_4 embedded in rotating medium (shown in Fig. 4(b)) is also virtually rotated into point b_3' in the virtual space. Therefore, the separation distance of two point sources (in Fig. 4(b)) in virtual space is just 0.25 λ, resulting in the undistinguishable of these two point sources (see the far field features of blue and green curves in Fig. 4(d)). Here, these two undistinguishable point sources in Fig. 4(b) show that they are nearly overlapped with each other due to the circular wavefront and far field feature of the corresponding field distribution (see Fig. 4(b) and blue curve in Fig. 4(d)). In theory, by reducing the thickness of the transformation medium, we can reduce the distance between point a_3' and b_3' to further realize the perfect overlapped optics. Therefore, the phenomenon demonstrated in Fig. 4(b) could be more or less categorized as the overlapping illusion.

Actually, both of the two phenomena, *i.e.*, super-resolution effects and overlapping illusion, are dependent on the separation distance of these two sources in real space and virtual space, respectively. For the super-resolution effects, the separation distance of the two point sources in the real space should be less than $\lambda/2$ while it should be larger than $\lambda/2$ in the virtual space, which means that $|a_4b_4| < \lambda/2$ and $|a_4b_3| > \lambda/2$, based on the Rayleigh criterion (due to the Abble diffraction limit). For the overlapping illusion, it also should meet the above conditions, which can be expressed as follows:

$$\begin{cases} \frac{\lambda}{2} > 0.25 \text{ mm} \\ \frac{\lambda}{2} < 0.778 \text{ mm} \end{cases} \rightarrow 0.778 \text{ mm} > \frac{\lambda}{2} > 0.25 \text{ mm}. \tag{6}$$

Therefore, the operating bandwidth of our proposed device is ranging from 0.1928 to 0.6 THz.

Although the effects of breaking diffraction limit and the overlapping illusion can be realized based on the homogeneous and anisotropic rotating medium, it is very hard to be found in nature and fabricated. So, we need to remove the anisotropic to further simplify the material parameters. Based on the effective medium theory, such homogeneous and anisotropic rotating medium can be replaced by alternating layered isotropic dielectrics, *i.e.*, two kinds of medium (medium A and medium B). The corresponding rotating angle of each layer is given as follows:

$$\alpha = (1/2)\tan^{-1}\left(\frac{2\varepsilon_{xy}}{\varepsilon_{xx}-\varepsilon_{yy}}\right) \tag{7}$$

$$\varepsilon_r^{A,B} = \zeta^1 \pm \sqrt{\zeta^1\left(\zeta^1-\zeta^2\right)} \tag{8}$$

where $\zeta^{1,2} = \left[\varepsilon_{xx}+\varepsilon_{yy} \pm \sqrt{\left(\varepsilon_{xx}-\varepsilon_{yy}\right)^2+4\varepsilon_{xy}^2}\right]/2.$

After detailed calculation, the layered material parameters are as follows:

For the inner triangle:

$$\varepsilon_r^B = 0.04843, \quad \varepsilon_r^B = 0.04843, \quad \mu_r^A = \mu_r^B = 1.0. \tag{9}$$

For the external triangle:

$$\varepsilon_r^A = 41.88690, \quad \varepsilon_r^B = 0.02387, \quad \mu_r^A = \mu_r^B = 1.0. \tag{10}$$

In what follows, we investigate the breaking of diffraction limit based on the homogeneous and isotropic layered transformation medium shown in Eqs. (7)–(10). Figs. 5(a) and 5(c) illustrate the magnetic field distribution of two separated identical point sources in free space and located at point a_4', b_4', and a_4, b_3 respectively. Fig. 5(b) shows the corresponding magnetic field distribution of two separated identical point sources located at point a_4', b_4', covered with the layered rotating

medium. The field distribution of Fig. 5(a) demonstrates the undistinguishable feature of two separated identical point sources (in free space) located at point a_4' and b_4' (see the far field pattern in Fig. 5(d) of blue curve). In contrast, these two separated identical point sources located at point a_4 and b_4 and coated with the layered rotating medium (see Fig. 5(b)) can further enhance the separation distance between each other. Therefore, the same field distribution of two separated point sources, with separation distance of 0.778 λ in the free space and shown in Fig. 5(c), indicates the effects of beyond diffraction limit. Figs. 5(b) and 5(c) also have the same far field features, indicating that two separated identical point sources, with a separation distance less than the 'differential limit', can also be broken based on the layered rotating medium. In addition, such layered rotating medium can also be extended to realize the overlapping illusion (not shown here).

4. Conclusion

In conclusion, we design a kind of pentagon field rotator, which can realize the effects of breaking diffraction limit as well as overlapping illusion, resulting in a tri-functional device. Based on effective medium theory, such a kind of homogeneous and anisotropic rotating medium can be replaced by homogeneous and isotropic alternating layered dielectrics. All of the above phenomena are demonstrated based on the two-dimensional finite element simulations. Both the theoretical model and numerical simulations provide us with a creative method for designing multifunctional transformation devices.

Acknowledgments

This work was supported in part by the National Program on Key Basic Research Project of China (973 Program) (2014CB339806), the Major National Development Project of Scientific Instrument and Equipment (2017YFF0106300, 2016YFF0100503), National Natural Science Foundation of China (61307126), the Key Scientific and Technological Project of Science and Technology Commission of Shanghai Municipality (15DZ0500102), Shanghai leading talent (2016-019), and Young Yangtse Rive Scholar (Q2016212). We would like to thank Prof. Yi Liu for his contribution to the manuscript.

References

[1] U. Leonhardt, Optical conformal mapping, Science 312 (2006) 1777–1780.
[2] J.B. Pendry, D. Schurig, D.R. Smith, Controlling electromagnetic fields, Science 312 (2006) 1780–1782.
[3] H.S. Chen, B.-I. Wu, B.L. Zhang, J.A. Kong, Electromagnetic wave interactions with a metamaterial cloak, Phys. Rev. Lett. 99 (2007) 063903.
[4] M. Rahm, D. Schurig, D.A. Roberts, S.A. Cummer, J.B. Pendry, Design of electromagnetic cloaks and concentrators using form-invariant coordinate transformations of Maxwell's equations, Photon. Nanostr. Fundam. Appl. 6 (2008) 87–95.
[5] W.X. Jiang, T.J. Cui, G.X. Yu, X.Q. Lin, Q. Cheng, J.Y. Chin, Arbitrarily elliptical-cylindrical invisible cloaking, J. Phys. D: Appl. Phys. 41 (2008) 085504.
[6] C. Li, F. Li, Two-dimensional electromagnetic cloaks with arbitrary geometries, Opt. Express 16 (2008) 13414–13420.
[7] C.W. Qiu, L. Hu, X. Xu, Y. Feng, Spherical cloaking with homogeneous isotropic multilayered structures, Phys. Rev. E 79 (2009) 047602.
[8] J. Li, J.B. Pendry, Hiding under the carpet: A new strategy for cloaking, Phys. Rev. Lett. 101 (2008) 203901.
[9] H. Ma, S. Qu, Z. Xu, J. Wang, The open cloak, Appl. Phys. Lett. 94 (2009) 103501.
[10] Y. Lai, H.Y. Chen, Z.Q. Zhang, C.T. Chan, Complementary media invisibility cloak that cloaks objects at a distance outside the cloaking shell, Phys. Rev. Lett. 102 (2009) 093901.
[11] T. Han, C.-W. Qiu, X.H. Tang, The general two-dimensional open-closed cloak with tunable inherent discontinuity and directional communication, Appl. Phys. Lett. 97 (2010) 124104.
[12] H. Gao, B. Zhang, G. Barbastanthis, H.D. Sun, Compact optical waveguide coupler using homogeneous uniaxial medium, J. Opt. Soc. Am. B. 28 (2011) 2633–2636.
[13] B. Zhang, Electrodynamics of transformation-based invisibility cloaking, Light: Sci. & Appl. 1 (2012) e32.
[14] T. Han, X. Bai, D. Gao, J.T.L. Thong, B. Li, C.-W. Qiu, Experimental demonstration of a bilayer thermal cloak, Phys. Rev. Lett. 112 (2014) 054302.
[15] H. Xu, X. Shi, F. Gao, H. Sun, B.L. Zhang, Untra-thin three-dimensional thermal cloak, Phys. Rev. Lett. 112 (2014) 054301.
[16] Y. Li, X. Shen, Z. Wu, J. Huang, Y. Chen, Y. Ni, J.P. Huang, Temperature-dependent transformation thermotics: From switchable thermal cloaks to macroscopic thermal diodes, Phys. Rev. Lett. 115 (2015) 195503.
[17] D. Schurig, J.J. Mock, J. Justice, S.A. Cummer, J.B. Pendry, A.F. Starr, D.R. Smith, Metamaterial electromagnetic cloak at microwave frequencies, Science 314 (2006) 977–980.
[18] R. Liu, C. Ji, J.J. Mock, J.Y. Chin, T.J. Cui, D.R. Smith, Broadband ground-plane cloak, Science 323 (2009) 366–36.
[19] J. Valentine, J. Li, T. Zentgraf, G. Bartal, X. Zhang, An optical cloak made of dieletric, Nature Mater. 8 (2009) 568–571.
[20] H.F. Ma, T.J. Cui, Three-dimensional broadband ground-plane cloak made of metamaterials, Nature Commun. 1 (2010) 21.
[21] B. Zhang, Y. Luo, X. Liu, G. Barbastathis, Macroscopic invisibility cloak for visible light, Phys. Rev. Lett. 106 (2011) 033901.
[22] D. Liang, J. Gu, J. Han, Y. Yang, S. Zhang, W. Zhang, Robust large dimension terahertz cloaking, Adv. Mater. 24 (2012) 916–921.
[23] H.S. Chen, B. Zheng, L. Shen, H. Wang, X. Zhang, N.I. Zheludev, B.L. Zhang, Ray-optics cloaking devices for large objects in incoherent natural light, Nature Commun. 4 (2013) 2652.
[24] M. Rahm, S.A. Cummer, D. Schurig, J.B. Pendry, D.R. Smith, Optical design of reflectionless complex media by finite embedded coordinate transformations, Phys. Rev. Lett. 100 (2008) 06390.
[25] Q. Cheng, T.J. Cui, W.X. Jiang, B.G. Cai, An omnidirectional electromagnetic absorber made of metamaterials, New J. Phys. 12 (2010) 063006.
[26] T. Yang, H.Y. Chen, X. Luo, H.R. Ma, Superscatterer: Enhancement of scattering with complementary media, Opt. Express 16 (2008) 18545–18550.
[27] H.Y. Chen, C.T. Chan, S. Liu, Z. Lin, A simple route to a tunable electromagnetic gateway, New J. Phys. 11 (2009) 083012.
[28] C. Li, X. Meng, X. Liu, F. Li, G. Fang, H.Y. Chen, C.T. Chan, Experiment realization of a circuit-based broadband illusion-optics analogue, Phys. Rev. Lett. 105 (2010) 233906.
[29] Y. Xu, S. Du, L. Gao, H.Y. Chen, Overlapped illusion optics: A perfect lens brings a brighter feature, New J. Phys. 13 (2011) 023010.
[30] J.J. Li, X.F. Zang, J.F. Mao, M. Tang, Y.M. Zhu, S.L. Zhuang, Overlapped optics induced perfect coherent effects, Sci. Rep. 3 (2013) 2569.
[31] X.F. Zang, C. Shi, Z. Li, L. Chen, B. Cai, Y.M. Zhu, H.B. Zhu, Illusion induced overlapped optics, Opt. Express 22 (2014) 582–592.
[32] W.X. Jiang, C.-W. Qiu, T.C. Han, Q. Cheng, H.F. Ma, T.J. Cui, Broadband all-dielectric magnifying lens for far-field high-resolution imaging, Adv. Mater. 25 (2014) 6963–6968.
[33] X.M. Li, W.S. Hua, X.Q. Wu, Research on optical antenna of ultraviolet communication based on two-surface reflection, Opt. Instrum. 34 (2012) 21–25 (2012).
[34] Y. Dong, Y. Zhang, W.S. Hua, Y. Chu, Stealth technology of photo-electric equipments based on the magneto-optical rotation effect, Opt. Instrum. 34 (2012) 80–85.
[35] Y. Du, X.F. Zang, C. Shi, X.B. Ji, Y.M. Zhu, Shifting media induced super-solution imaging, J. Opt. 17 (2015) 025606.
[36] F. Sun, S.L. He, Overlapping illusions by transformation optics without any negative refraction material, Sci. Rep. 6 (2016) 19130.
[37] H.Y. Chen, C.T. Chan, Transformation media that rotate electromagnetic fields, Appl. Phys. Lett. 91 (2007) 183518.
[38] . Hu. Y. Chen, B. Hou, S. Chen, X. Ao, W. Wen, C.T. Chan, Design and experimental realization of a broadband transformation media field rotator at microwave frequencies, Phys. Rev. Lett. 102 (2009) 183903.
[39] G. Liu, C. Li, C. Chen, Z. Lu, G. Fang, Experimental verification of field rotating with invisibility by full tensor transmission-line metamaterials, Appl. Phys. Lett. 101 (2012) 224105.
[40] T. Han, Z. Wu, Electromagnetic wave rotators with homogeneous nonmagnetic, and isotropic materials, Opt. Lett. 39 (2014) 3689–3692.
[41] X.F. Zang, Y.M. Zhu, X.B. Ji, L. Chen, Q. Hu, S.L. Zhuang, Broadband unidirectional behavior of electromagnetic waves based on transformation optics, Sci. Rep. 7 (2017) 40941.
[42] R. Liu, C. Ji, J.J. Mock, J.Y. Chin, T.J. Cui, D.R. Smith, Broadband ground-plane cloak, Science 323 (2009) 366–369.
[43] H.F. Ma, T.J. Cui, Three-dimensional broadband and broad-angle transformation-optics lens, Nature Commun. 1 (2010) 124.
[44] L. Xu, H.Y. Chen, Conformal transformation optics, Nature Photon. 9 (2015) 15–23.
[45] X. Chen, Y. Luo, J. Zhang, K. Jiang, J.B. Pendry, S. Zhang, Macroscopic invisibility cloaking of visible light, Nature Commun. 2 (2011) 176.
[46] D. Schurig, J.B. Pendry, D.R. Smith, Calculation of material properties and ray tracing in transformation media, Opt. Express 14 (2006) 9794–9804.